Experimental analysis and modeling of the anisotropic response of titanium alloy Ti-X for quasi-static loading at room temperature

M. Tritschler[a,]*, A. Butz[a], D. Helm[a], G. Falkinger[a], J. Kiese[b]

[a] *Fraunhofer-Institute for Mechanics of Materials IWM, 79108 Freiburg, Germany*
[b] *ThyssenKrupp VDM GmbH, 45143 Essen, Germany*

* Corresponding author. Tel.: +49 761 5142 479; fax: +49 761 5142 510.
E-mail adress: matthias.tritschler@iwm.fraunhofer.de (M. Tritschler).

Keywords:

Titanium, Anisotropy, Tension-Compression Asymmetry, Bauschinger effect, Springback

Abstract

The present paper deals with the characterization and modeling of the deformation behavior of titanium alloy Ti-X© under quasi-static conditions at room temperature. The material investigated is a rolled sheet of thickness 1.2 mm with a strong basal texture. In order to characterize the material behavior, monotonic tensile, compression and cyclic tests in different directions with respect the rolling direction were conducted. Texture information was obtained from electron backscatter diffraction (EBSD) data. Furthermore, strip drawing tests were carried out. Using the visco-plastic self-consistent texture model (VPSC) the experimental data have been extended to biaxial stress states. To describe the yield surface, the CPB06ex2 model (Plunkett et al., 2008) was used. This model can describe the anisotropy and the tension-compression asymmetry. Considering the evolution of the model parameters, anisotropic hardening could be described. An extension of the model with the approach of Armstrong and Frederick offers the possibility to account for the Bauschinger effect during cyclic loading. A very good agreement between FE simulation and experimental data was obtained.

1. Introduction

Because of their outstanding properties such as the favorable ratio between weight and strength, good ductility, high heat resistance, corrosion resistance and biocompatibility, titanium and its alloys are ideal materials for aerospace, medical engineering, chemical industry, and many other high-tech areas.
In recent years, considerable efforts were undertaken to characterize and to model the response of titanium and its alloys (see for example, Follansbee and Gray, 1989; Nemat-Nasser et al., 1999, 2001, Majorell et al., 2002, Kahn et al., 2004). The focus of these studies lay on the characterization and modeling of the uniaxial behavior at different strain rates and temperatures. However, the material is exposed to multiaxial loading during processing, which leads to a more complex response. So Kahn et al. (2007) dealt with the characterization and modeling of multiaxial loading conditions. Many studies dealt with the plastic deformation mechanisms (see for example, Lecomte et al., 1997; Yapici et al., 2006; Seshacharyulu et al., 2000, 2002). It turned out that, as in other hexagonal materials, twinning plays an important role besides slip. In contrast to dislocation slip, twinning is direction-dependent, which may lead to a pronounced tension-compression asymmetry (Cazacu et al., 2006). It has been shown that classical phenomenological plasticity models using von Mises or Hill'48 yield potentials are not capable of describing this asymmetry (see for example,

Nixon et al., 2010). In addition to the tension-compression asymmetry, anisotropic hardening also occurs in titanium and its alloys.
Anisotropic formulations at the macroscopic level offer an approach for the description of the material behavior. These formulations have the advantage that they can be easily implemented into a finite element code and can easily be applied in calculations of complex forming processes. In recent years, for materials with cubic crystal structure significant progress has been made in the development of mathematical descriptions of anisotropic yield surfaces. In Cazacu and Barlat (2001, 2003) for example, the isotropic yield function of Drucker has been extended to an anisotropic yield function which describes the response of aluminum alloys. Furthermore, for three-dimensional stress states flow functions were developed, which are capable of describing the initial anisotropy and the tension-compression asymmetry. Thus, in Cazacu and Barlat (2004) an isotropic yield function has been extended to the anisotropic case by generalizing the invariants. The comparison between this yield function and experimental data for the hexagonal material magnesium showed that this model is capable of describing the anisotropy and the tension-compression asymmetry. In Cazacu et al. (2006) another yield function has been presented, which describes asymmetric yielding between tension and compression due to twinning. In a further step this yield function has been extended to cover also the anisotropy. For this purpose the stress deviator has been linearly transformed with a fourth-order tensor. This model was applied to magnesium and titanium alloys and showed a high degree of accuracy. In Plunkett et al. (2008) it is shown that this accuracy can be increased by carrying out two or more linear transformations. However, the consideration of further linear transformations requires additional model parameters. One way to describe the anisotropic hardening is presented in Plunkett et al. (2006). For certain values of equivalent plastic strain the coefficients of the yield function were determined from experimental data. In a further step the equivalent stress is calculated. For strains that are located between two grid points, it is interpolated linearly between the calculated equivalent stresses. With this approach the shape of the yield surface in stress space is capable to evolve. Another important aspect is the description of the material under cyclic loading. Especially in deep drawing processes the material undergoes a cyclic loading, which has a significant influence on the springback behavior of deep-drawn components. Therefore the description of the Bauschinger effect, connected with the cyclic loading, plays a central role to properly reflect the material response. One approach to this is the model of Armstrong and Frederick (1966).
In the present study (Section 2) the results of different experimental investigations will be presented. The aim was to characterize the material under quasi-static conditions at room temperature. In addition to standard tensile, compression and cyclic tests, the texture was measured using electron backscatter diffraction (EBSD). Furthermore, a simple deep drawing test was carried out, a so-called “strip drawing test”. This test includes all the essential elements of a conventional deep drawing process and is suitable to investigate the springback behavior of the material. In Section 3, with the help of the visco-plastic self-consistent texture model (VPSC) (see Lebensohn and Tomé, 1993), the material behavior under biaxial stress states is analyzed in order to generate numerical data additional to the experimental data base. This information about the material behavior is used for introducing a finite plasticity model with an appropriate yield function and to identify the material parameters (Section 4). For representing the evolving plastic anisotropy, the yield function CPB06ex2 (see Plunkett et al., 2008) is applied. This model is suitable to describe processes in which due to a monotonic loading history the isotropic hardening is significant, for example in a hydroforming process. In deep drawing processes not only isotropic hardening but also kinematic hardening is relevant, due to cyclic deformation. For this reason, the material model is enhanced by a backstress tensor for modeling the kinematic hardening. Finally, numerical studies on simple sheet metal forming processes are used to demonstrate the capability of the model for representing the material behavior of Ti-X.

2. Experimental procedures

2.1 Material

The titanium alloy used in this study was Ti-X. This alloy is a new development by ThyssenKrupp VDM GmbH and was supplied in the form of a rolled sheet with thickness 1.2 mm. The physical properties of this alloy are comparable with those of Ti-Grade 2. The composition can be found in table 1.

Table 1: Chemical composition of the Ti-X alloy in weight-% [wt%].

Ti	Si	Fe	RE	O_2
base material	0.3	0.1	0.2	0.06

RE: rare earth, Cerium misch metal

The alloying of silicon and iron increases the oxidation resistance. Both the rare earth and cerium misch metal lead to a lowering of the strength. In contrast to commercially pure titanium this alloy can be used up to 900 °C. Hence, this alloy is suitable for the use in exhaust systems. According to Boyer et al., 1994, the density is about $\rho = 4.51$ g/cm^3, the Poisson's ratio between $\nu = 0.28$ to 0.34 and the Young's modulus E = 103000 MPa. It should be noted that the Young's modulus of sheet metals depends on the orientation with respect to the rolling direction, as shown in Section 2.2.3. The beta-transus temperature is typically 910 °C.

Investigations with optical microscopy showed that the material has a globular microstructure (Fig. 1). The average grain size is about 10 µm. Electron backscatter diffraction (EBSD) measurements showed that the as received rolled sheet exhibits a strong basal texture (Figs. 2).

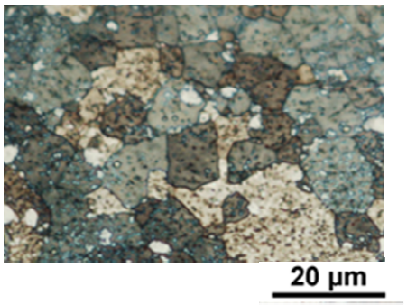

Fig. 1: Micrograph of the titanium alloy Ti-X.

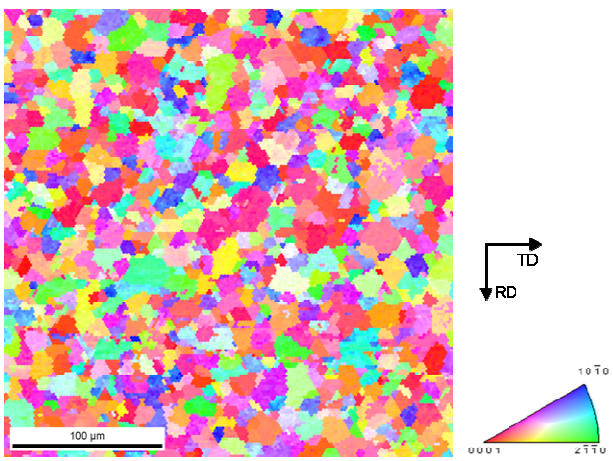

Fig. 2: Inverse pole figure.

2.2 Quasi-static behavior of Ti-X

2.2.1 Tensile tests at room temperature

To characterize the sheet metal under quasi-static conditions, tensile tests in three different directions to the rolling direction (0°, 45°, 90°) at room temperature were conducted. These experiments were performed on a universal testing machine (INSTRON 8861) with a 100 kN load cell. The specimens were cut from the sheet using Electrical Discharge Machining (EDM) to avoid changes in the material due machining. Fig. 3 shows the geometry and the dimensions of the specimens used for in-plane uniaxial tensile testing.

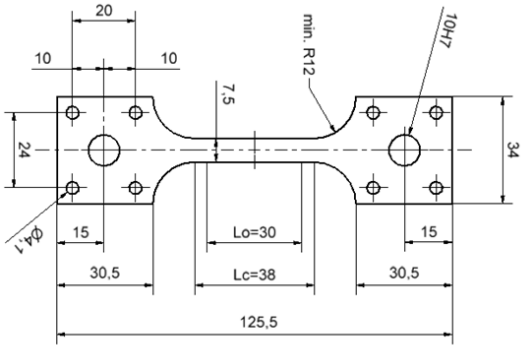

Fig. 3: Geometry und dimensions (in mm) of the specimens. Thickness t = 1.2 mm.

The tensile tests were performed at a crosshead speed of v = 0.02 mm/s up to failure. As shown in Fig. 3 the gauge length of the extensometer was L_0 = 30 mm. During the experiment, force and displacement in longitudinal and transverse directions were recorded. The displacement in longitudinal direction was measured by an extensometer while the displacement in transverse direction was measured optically. In addition to the stress-strain curves, the r-values were also calculated. To ensure the reproducibility of the experiments, three trials per test direction were carried out.

2.2.2 Compression and tension-compression tests at room temperature

Compression and tension-compression tests were conducted to characterize the well-known tension-compression asymmetry as well as the cyclic behavior of titanium. The data from the cyclic tests are used to fit the parameters of the Armstrong and Frederick model. By Electrical Discharge Machining (EDM) the specimens were cut in three different directions to the rolling direction (0°, 45° and 90°). In Fig. 4, the geometry and the dimensions of the specimens are shown. To avoid buckling of the specimen an appropriate ratio between width and thickness is chosen. This leads to a gauge length of the extensometer of L_0 = 1.3 mm.

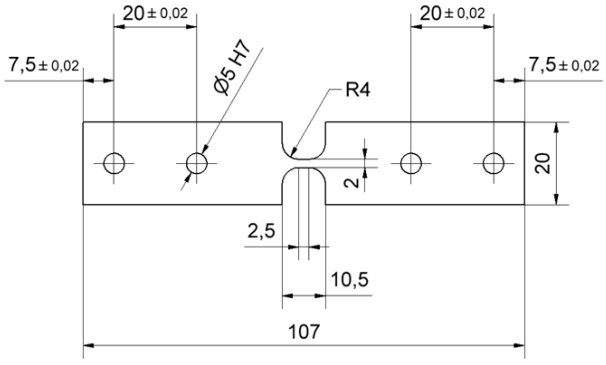

Fig. 4: Geometry and dimensions (in mm) of the specimens. Thickness t = 1.2 mm.

The compression and the tension-compression tests were performed with a special device on an INSTRON 1380/2 (Fig. 5). A very precise clamping tool, rigid sample holder and a small gauge length prevent buckling of the specimens in the compression range. Due to the commencement of bulging, the tests could only be run up to 4 % plastic strain in the compression range. For the compression tests, two trials per specimen orientation were carried out. In the same way two trials per test direction were conducted for the tension-compression and compression-tension test respectively. This should detect whether the sequence of the loading directions, i.e. tension or compression first, has a relevant influence on the resulting cyclic stress-strain curves.

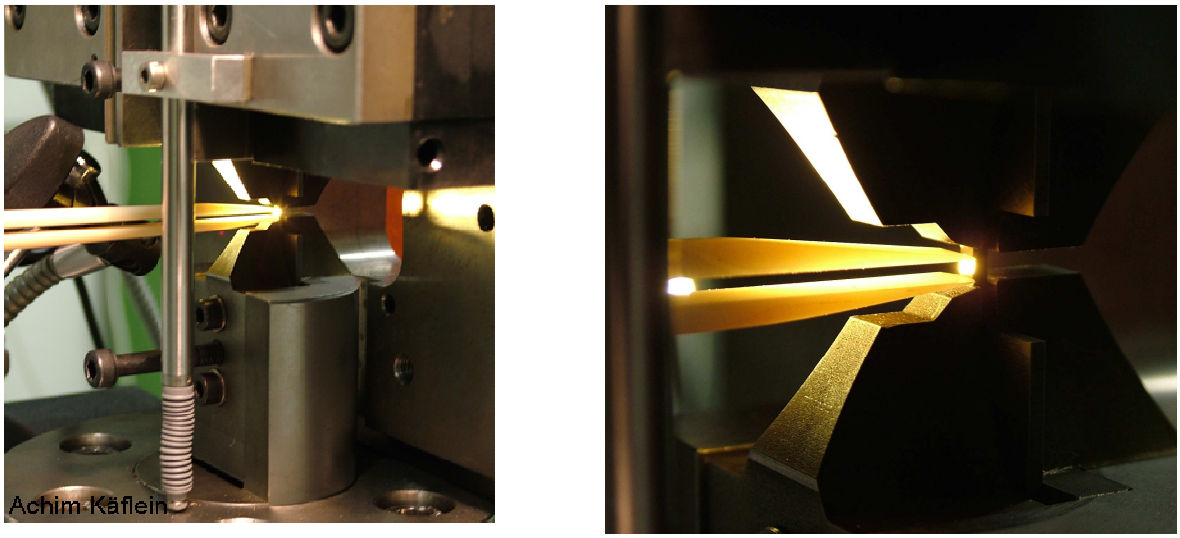

Fig. 5: Experimental setup for compression and tension-compression experiments (left), detail (right).

2.2.3 Results

Fig. 6 shows the true stress-strain curves measured in tensile tests before the onset of necking. In addition to the different initial flow stresses the material also exhibits anisotropic hardening and significant differences in the r-values. The experiments are reproducible. Table 2 lists some characteristic values of this material.

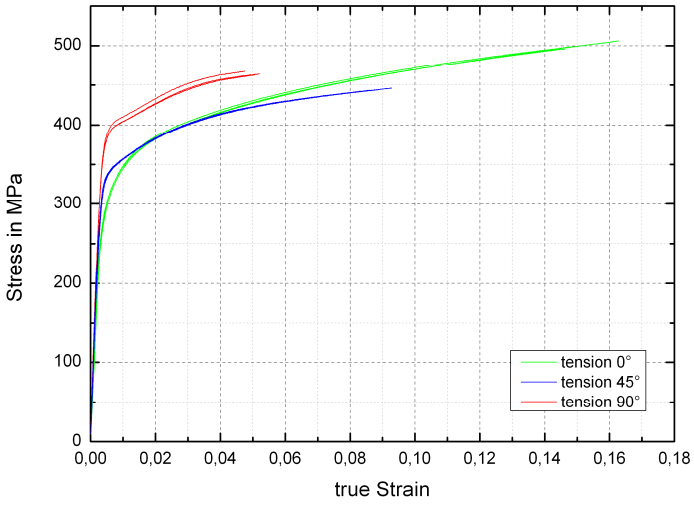

Fig. 6: Tensile tests in 0°, 45° and 90° to the rolling direction at room temperature.

Table 2: Technical values at room temperature.

test direction	0°	45°	90°
$R_{p0,2}$ [MPa]	297	333	384
R_m [MPa]	430	407	442
A_g [%]	16,08	8,97	4,77
A_{30} [%]	37,77	40,33	33,17
Young's-modulus [GPa]	100	108	116
r-value [-]	1,06	2,36	3,3

The compression tests show anisotropy of the initial yield stress, while, there is an almost equally strong strain hardening in the investigated strain range (Fig. 7). A comparison between the tensile and compression tests shows the tension-compression asymmetry, typical for hexagonal materials with this texture. Due to the commencement of a kink, the data were recorded only up to 4 % plastic strain. Again, the experiments were reproducible.

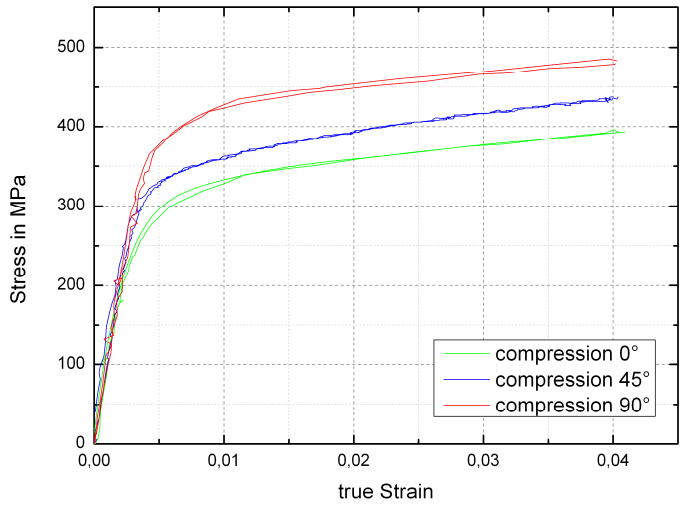

Fig. 7: Compression tests in 0°, 45° and 90° to the rolling direction at room temperature.

In Fig. 8 A-C the measured cyclic stress-strain curves for three cycles are shown. The experiments were carried out up to a strain amplitude of 4%. A very good reproducibility was observed. In all experiments a pronounced Bauschinger effect is visible, regardless of the orientation.

A: *Cyclic test in 0° direction*

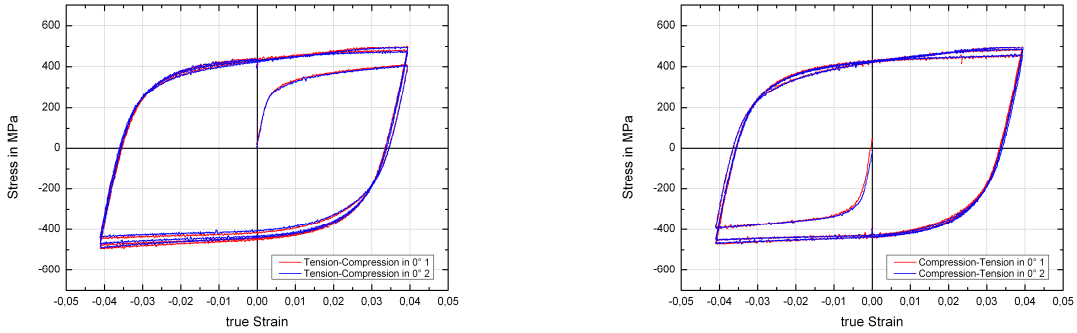

B: *Cyclic test in 45° direction*

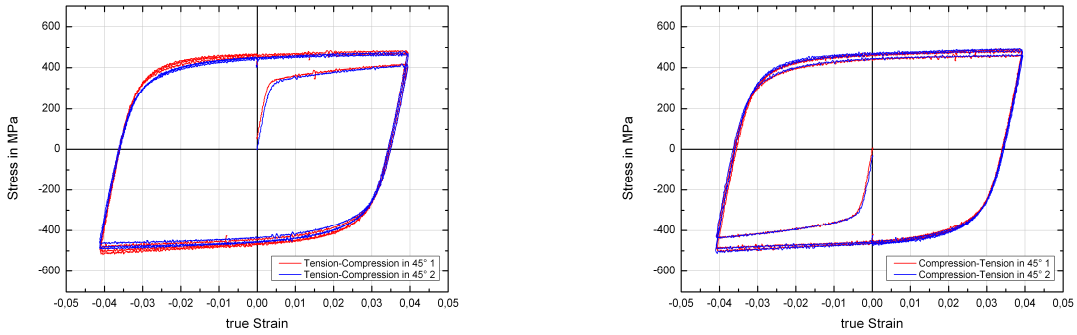

C: *Cyclic test in 90° direction*

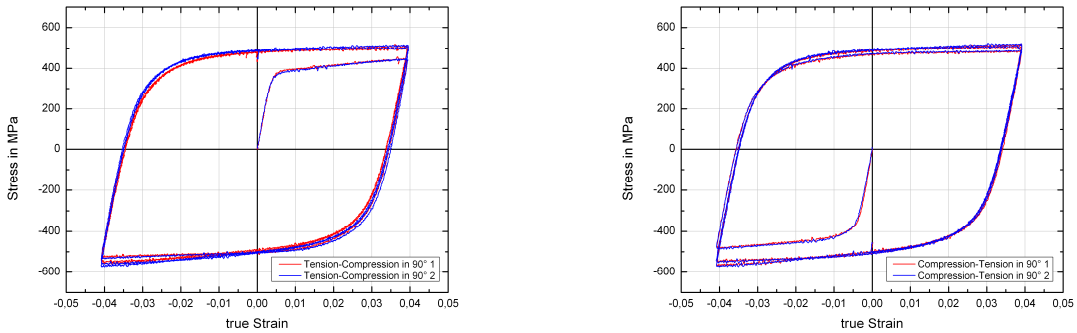

Fig. 8: Cyclic tests in different directions with strain amplitude of 4%.

2.2.4 Strip drawing test at room temperature

To investigate the springback characteristics of the studied material, a so-called strip drawing test was performed. This test includes the essential elements of a conventional deep drawing process. The experimental setup is shown in Fig. 9. A sheet metal strip with a width of 30 mm and a length of 348 mm is tested. In a first step, the blank holder presses the strip against the die with a force of 4 kN. This corresponds to a pressure of 3 MPa. The blank holder force controls the flow of material and was chosen such that the sheet did not fail when entering the die. Then a punch draws the sheet into the die (punch stroke of 60 mm), thus forming a hat profile (see Fig. 10 left). After removing punch and blank holder the strip springs back (see Fig. 10 right). The design of the tool allows the variation of the die radius, the drawing gap between the die and the punch and the blank holder force. In the studies of this work a die radius of 5 mm is used. To reduce the friction between blank holder, die and sheet, a standard deep drawing oil (KMT80) is used.

The springback is an important reference for the evaluation of the used material model with anisotropic-kinematic hardening.

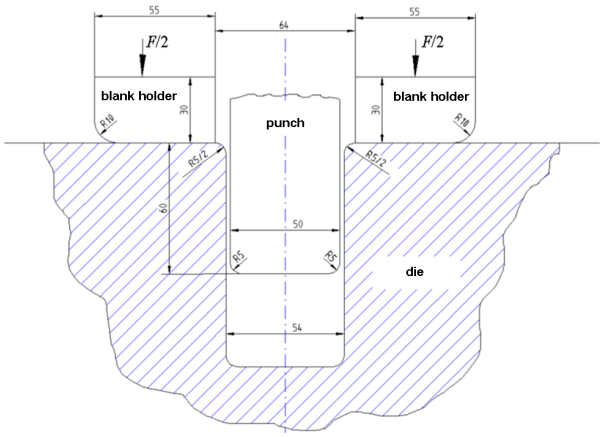

Fig. 9: Section through the experimental setup of the strip drawing test (Krasovskyy, 2005).

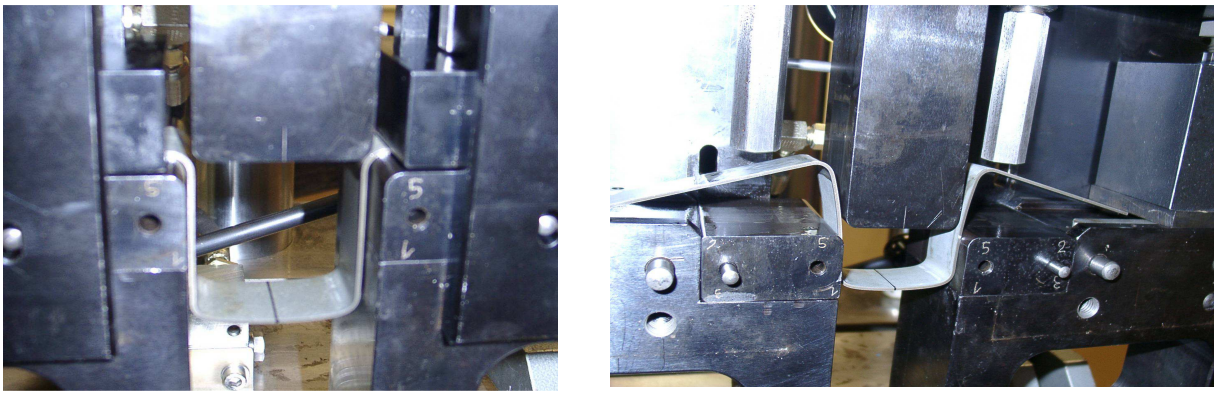

Fig. 10: Deep drawing process (left), shape after springback (right).

3. Polycrystal model

As mentioned before, the uniaxial standard tests are supplemented by using simulation results of the visco-plastic self-consistent texture model (VPSC). Therefore, biaxial stress states, i.e. biaxial tension and biaxial compression, are investigated by virtual tests. In this model, each grain is regarded as an anisotropic, viscoplastic, ellipsoidal inclusion embedded in a homogeneous equivalent medium. Therefore, the information about the orientation and the volume fraction of grains must be available. The homogeneous equivalent medium represents the average properties of all the other grains. There is a stress-strain coupling between grain and medium. The plastic deformation behavior of the grain is calculated on the basis of single crystal plasticity. By considering the crystal lattice orientation and the rotation due to an external load, the anisotropy and its evolution can be described. By homogenization of the calculated strains and stresses of each grain, the macroscopic response of the material is produced. A modified Voce model is used to describe the hardening behavior on a slip plane (Eq. (1)):

$$\tau_c^s = \tau_0^s + \left(\tau_1^s + \theta_1^s \Gamma\right) \cdot \left(1 - e^{-\Gamma \theta_0^s / \tau_1^s}\right). \quad (1)$$

Here τ_c^s is the critical shear stress of the sliding system *s*, Γ the accumulated strain and τ_0^s, τ_1^s, θ_0^s, as well as θ_1^s are model parameters. A detailed description of the model can be found in the original article (Lebensohn and Tomé, 1993).

To perform the VPSC simulations, the initial texture shown in Fig. 2 was used; 1509 grains were considered in the simulations. The parameters for the Voce hardening law were fitted by hand to experimental data (tension in 0° and 90° and compression in 0°). It was assumed that plastic deformation occurs due to prismatic, basal, and pyramidal <c+a> slip systems as well as twinning. Figs. 11 and 12 show the fitted stress-strain curves and Table 3 shows the fitted hardening parameters. The strain rate exponent *n* is set to 20 to ensure an approximately rate-independent behavior. For the material under investigation, the characteristic twin shear has a value of 0.169.

Table 3: Hardening parameters for Voce law.

Mode	τ_0	τ_1	θ_0	θ_1
Prismatic	110	60	2000	190
Basal	220	60	2600	10
Pyramidal <c+a>	450	1	1	1
Tensile twinning	250	35	600	0

To assess the quality of the determined model parameters, a compression test in 90° was simulated. As shown in Fig. 12, the model could predict the experimental curve well. In addition, the r-values in 0°, 45° and 90° were simulated with this parameter set and compared with the experimental values (Table 4). Again, the agreement was very good.

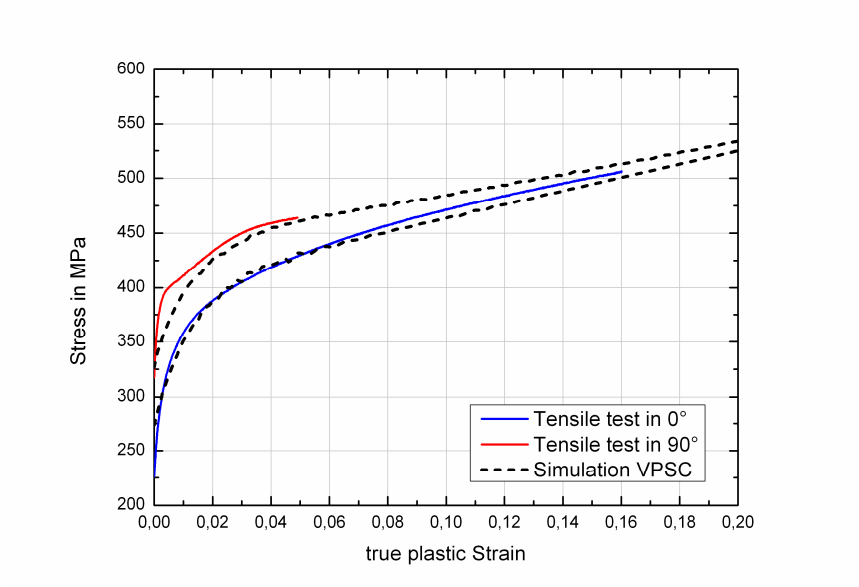

Fig. 11: Comparison between VPSC simulation and experimental data for tensile tests.

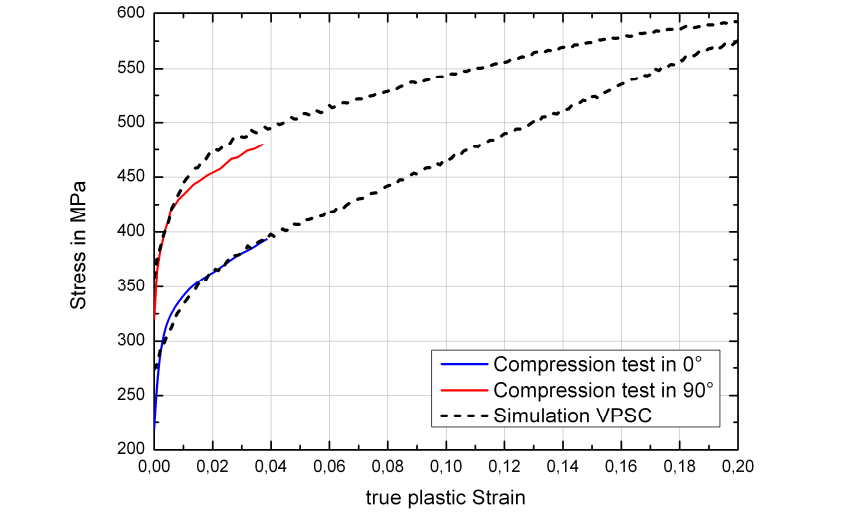

Fig. 12: Comparison between VPSC simulation and experimental data for compression tests.

Table 4: Comparison of the r-values between VPSC simulation and experimental data.

	0°	45°	90°
Experimental data	1,06	2,36	3,3
VPSC simulation	1,04	2,31	3,3

In a further step, the predictive accuracy of the VPSC model was checked with respect to the texture development. Thereto a tensile test up to a true plastic strain of 10.5 % was performed and the texture was measured using EBSD. In Fig. 13 the measured pole figures are compared with pole figures calculated with the VPSC model. The qualitative features are consistent, while the predicted intensities are slightly too high. Thus, after these validations it can be assumed that the used parameter set is suitable to describe the behavior of the material under multiaxial loading. On this basis, biaxial stress states in tension and compression were simulated.

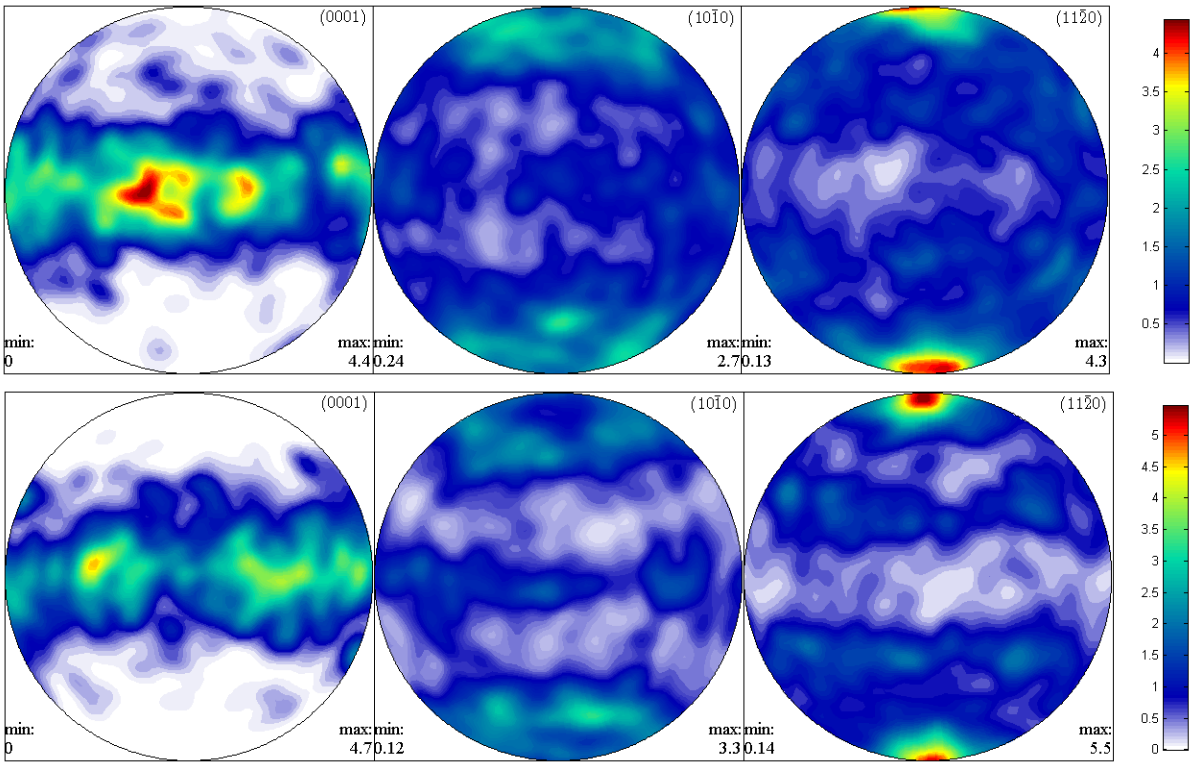

Fig. 13: Texture at 10.5 % plastic strain, above: experimental data from EBSD, below: VPSC simulation.

4. Macroscopic model

On the macroscopic level the anisotropic yield locus and the hardening behavior are described using the anisotropic yield function CPB06ex2 after Plunkett et al., 2008. This model is briefly described below.

4.1 Material model

In the co-rotational framework, the strain rate tensor is additively decomposed into an elastic and a plastic part (see for example Han et al., 2003, Kahn and Huang, 1995, Wu et al., 2003)

$$\hat{\mathbf{D}} = \hat{\mathbf{D}}_e + \hat{\mathbf{D}}_p \,. \tag{2}$$

Furthermore, a hypo-elastic model is used, in which the stress-strain relationship in the elastic region is given by

$$\dot{\boldsymbol{\sigma}} = \mathbf{E}[\hat{\mathbf{D}} - \hat{\mathbf{D}}_p], \tag{3}$$

where **E** denotes the fourth-order elasticity tensor. The flow potential is defined as

$$F(\boldsymbol{\sigma}, \bar{\varepsilon}_{pl}) = \bar{\sigma}(\boldsymbol{\sigma}, \bar{\varepsilon}_{pl}) - Y(\bar{\varepsilon}_{pl}) \,. \tag{4}$$

Therein, $\bar{\sigma}$ is the equivalent stress as a function of the stress tensor and the equivalent plastic strain and Y is the reference stress as a function of the equivalent plastic strain. The reference stress is determined experimentally, for example by a uniaxial tensile test. Plastic flow begins when the yield condition (Eq. 5) and the loading condition is satisfied:

$$F(\boldsymbol{\sigma}, \bar{\varepsilon}_{pl}) = 0 \,. \tag{5}$$

The evolution of the plastic strain is given by the associated flow rule

$$\hat{\mathbf{D}}_p = \dot{\lambda} \frac{\partial F}{\partial \boldsymbol{\sigma}}, \tag{6}$$

where $\dot{\lambda}$ denotes the plastic multiplier. From the work-equivalence principle

$$\dot{W}_{pl} = \dot{\bar{\varepsilon}}_{pl} \bar{\sigma}\left(\boldsymbol{\sigma}, \bar{\varepsilon}_{pl}\right) = \hat{\mathbf{D}}_p \cdot \boldsymbol{\sigma} \tag{7}$$

follows the relationship between the equivalent plastic strain rate and the increment of the plastic multiplier:

$$\dot{\bar{\varepsilon}}_{pl} = \dot{\lambda} \,. \tag{8}$$

The equivalent stress is written in the form

$$\bar{\sigma} = B \cdot [f]^{1/a}, \tag{9}$$

where B is a constant defined such that the equivalent stress in the preferred direction (e.g. the rolling direction) reduces to the reference stress (Plunkett et al., 2006). The yield function f has the form

$$f = \left(\left|\Sigma_1\right| - k\Sigma_1\right)^a + \left(\left|\Sigma_2\right| - k\Sigma_2\right)^a + \left(\left|\Sigma_3\right| - k\Sigma_3\right)^a + \left(\left|\Sigma_1'\right| - k'\Sigma_1'\right)^a + \left(\left|\Sigma_2'\right| - k'\Sigma_2'\right)^a + \left(\left|\Sigma_3'\right| - k'\Sigma_3'\right)^a . \quad (10)$$

The tension-compression asymmetry can be described by k and k'. The parameter a represents the degree of homogeneity, and $\boldsymbol{\Sigma}$ and $\boldsymbol{\Sigma}'$ are linear transformations of the stress deviator **S** and are defined as follows:

$$\boldsymbol{\Sigma} = \mathbf{C} : \mathbf{S} \text{ and } \boldsymbol{\Sigma}' = \mathbf{C}' : \mathbf{S}, \quad (11)$$

where the stress deviator **S** is determined by

$$\mathbf{S} = \boldsymbol{\sigma} - \frac{1}{3}\left(\sigma_{11} + \sigma_{22} + \sigma_{33}\right). \quad (12)$$

Σ_1, Σ_2, Σ_3, Σ_1', Σ_2', and Σ_3' are the principal stresses of the transformed stress deviator. The fourth-order transformation tensors **C** and **C'** are represented in matrix notation by $\underline{\underline{\mathbf{C}}}$ and $\underline{\underline{\mathbf{C}}}'$

$$\underline{\underline{\mathbf{C}}} = \begin{bmatrix} C_{11} & C_{12} & C_{13} & 0 & 0 & 0 \\ C_{21} & C_{22} & C_{23} & 0 & 0 & 0 \\ C_{31} & C_{32} & C_{33} & 0 & 0 & 0 \\ 0 & 0 & 0 & C_{44} & 0 & 0 \\ 0 & 0 & 0 & 0 & C_{55} & 0 \\ 0 & 0 & 0 & 0 & 0 & C_{66} \end{bmatrix} \text{ and } \underline{\underline{\mathbf{C}}}' = \begin{bmatrix} C_{11}' & C_{12}' & C_{13}' & 0 & 0 & 0 \\ C_{21}' & C_{22}' & C_{23}' & 0 & 0 & 0 \\ C_{31}' & C_{32}' & C_{33}' & 0 & 0 & 0 \\ 0 & 0 & 0 & C_{44}' & 0 & 0 \\ 0 & 0 & 0 & 0 & C_{55}' & 0 \\ 0 & 0 & 0 & 0 & 0 & C_{66}' \end{bmatrix}. \quad (13)$$

For $k \in [-1, 1]$ and $a \geq 1$ the anisotropic yield function is convex. **C**, **C'**, a, k and k' are model parameters, which are fitted based on experimentally determined flow curves for monotonic tensile and compression tests in different directions relative to the rolling direction, r-values in different directions and further tests such as bulge tests. For $C_{ii} = 1$ and $C_{ij} = 0$ ($i \neq j$), $k = k' = 0$ and $a = 2$ the yield function reduces to the isotropic yield function.

With this model we are able to describe an anisotropic yield surface. Due to texture evolution the yield surface changes its shape with increasing equivalent plastic strain. To account for this effect in the model, a set of parameters must be determined for a certain number of values of the equivalent plastic strain. Between these reference points, the stress is linearly interpolated. For more information on this procedure see Plunkett et al. (2006) and Nixon et al. (2010). It has been shown that the proposed yield function can represent the yield surface of titanium alloys for monotonic loading paths with high accuracy.

4.2 Application of the proposed model to the titanium alloy Ti-X

4.2.1 Parameter fitting

The experimental data used for the parameter fitting come from tension and compression tests as well as r-values in three different directions to the rolling direction. For this material the

uniform elongations are relatively small. This means that there is information about the material behavior only for small strains. In view of the simulation of deep drawing processes, this database is not sufficient. Therefore, it is necessary to extrapolate the experimental data to larger strains. In this study simple strain dependent hardening models were used. The extrapolated data were also considered in the fitting procedure. Furthermore, the results of VPSC simulations for biaxial stress states were also taken into account. Based on this database, the anisotropy coefficients lying in the sheet plane were fitted (C_{ij} für i, j ≤ 4 und k). For this purpose the flow potential has to be formulated for the stress states to be fitted. This leads to the following equations:

$$\sigma_\theta^{T,C,biAx*} = \frac{1}{\bar{\sigma}(C_{ij}, C_{ij}^{'}, k, k^{'})} Y_{ref}\,, \tag{14}$$

$$r_\theta = \frac{\sin^2\theta \frac{\partial F}{\partial \sigma_{xx}} - \sin(2\theta)\frac{\partial F}{\partial \sigma_{xy}} + \cos^2\theta \frac{\partial F}{\partial \sigma_{yy}}}{-\left(\frac{\partial F}{\partial \sigma_{xx}} + \frac{\partial F}{\partial \sigma_{yy}}\right)} \tag{15}$$

with $0° \le \theta \le 90°$ (Plunkett et al., 2008).

The model parameters can be determined by minimizing an error function (Nixon et al., 2010) of the form

$$E\left(C_{ij}, C_{ij}^{'}, k, k^{'}\right) = \sum_k \left(\frac{\sigma_\theta^T}{\sigma_\theta^{\exp}} - 1\right)^2 + \sum_l \left(\frac{\sigma_\theta^C}{\sigma_\theta^{\exp}} - 1\right)^2 + \sum_m \left(\frac{r_\theta^T}{r_\theta^{\exp}} - 1\right)^2 + \sum_n \left(\frac{\sigma^{biAx}}{\sigma^{\exp}} - 1\right)^2 \tag{16}$$

**T:= Tension, C:= Compression, biAx:= biaxial stress state*

for i, j ≤ 4. The parameters k, l, m, n stand for the number of experimental data points. The experimental data were equally weighted. The anisotropy coefficients C_{55}, C_{66}, C'_{55} and C'_{66} which are associated with out-of-plane properties were set to the isotropic values (i.e. unity), because no experimental data were available. Assuming a plane stress condition as it is usual for sheet metals, this is justified. The degree of homogeneity was set to a = 5.
A successful parameter fitting procedure requires that the initial parameter set is appropriate because usually the minimum square error is a local minimum. This means that the model parameters are not unique. It has turned out to be helpful to take the isotropic case as a starting parameter set, i.e. to set the diagonal entries of the transformation tensor to the value 1 and all other parameters to the value 0 (except parameter a). The calculated parameters are listed in Table 5 for a fixed value of the equivalent plastic strain.

Table 5: Coefficients for the yield function CPB06ex2 for Ti-X corresponding to fixed values of the equivalent plastic strain.

$\bar{\varepsilon}_{pl}$	0%	1%	4%	10%	16%	20%
C_{11}	2,2703	4,9825	3,2303	3,6414	4,4904	4,8760
C_{22}	1,7865	0,0728	0,9109	2,1066	2,9378	3,4260
C_{33}	1,3511	2,8806	2,0464	2,8788	3,8952	4,4659
C_{44}	2,3264	4,2674	2,8350	3,7434	4,5385	4,9353
C_{55}	1	1	1	1	1	1
C_{66}	1	1	1	1	1	1
C_{12}	-0,1178	0,1174	-0,4448	-0,9595	-1,2630	-1,5533

C_{13}	-0,3976	1,4200	0,7389	0,9459	1,3924	1,5741
C_{23}	0,6981	-0,9042	-0,8541	-0,7793	-0,7103	-0,7051
k	0,0586	0,0733	0,0855	0,1228	0,1817	0,2646

$\bar{\varepsilon}_{pl}$	0%	1%	4%	10%	16%	20%
C'_{11}	2,2819	2,6113	1,8666	2,1220	2,8020	3,1050
C'_{22}	1,6307	-2,2333	-1,5571	-0,1821	-0,0122	-0,0105
C'_{33}	1,6250	2,2883	1,8577	2,1274	2,7466	2,9793
C'_{44}	0,0596	3,1070	2,6287	2,7399	3,6048	3,9002
C'_{55}	1	1	1	1	1	1
C'_{66}	1	1	1	1	1	1
C'_{12}	0,0573	0,4731	0,1926	0,1283	0,1566	0,2393
C'_{13}	0,4264	-0,9170	-0,6090	-0,5049	-0,4534	-0,2991
C'_{23}	-0,0049	-0,2775	0,1745	0,1345	0,0476	0,0422
k'	-0,0817	-0,2751	-0,3434	-0,6025	-0,6549	-0,8687

Fig. 14 (left) shows the yield loci of CPB06ex2 in the plane stress space corresponding to the parameters of Table 5. It can be seen that the shape of the yield locus evolves with increasing strain. Furthermore, the model accurately describes the experimental as well as the extrapolated data points and those simulated with VPSC. In Fig. 14 (right), the yield loci of von Mises, Hill'48 and CPB06ex2 at 0 % and 20 % equivalent plastic strain are shown for comparison. It can be seen that the models of von Mises and Hill'48 are not able to describe the material behavior with acceptable accuracy. Especially for biaxial stress, these models cannot reproduce the available data, although this stress state is particularly important for the simulation of sheet metal forming processes.

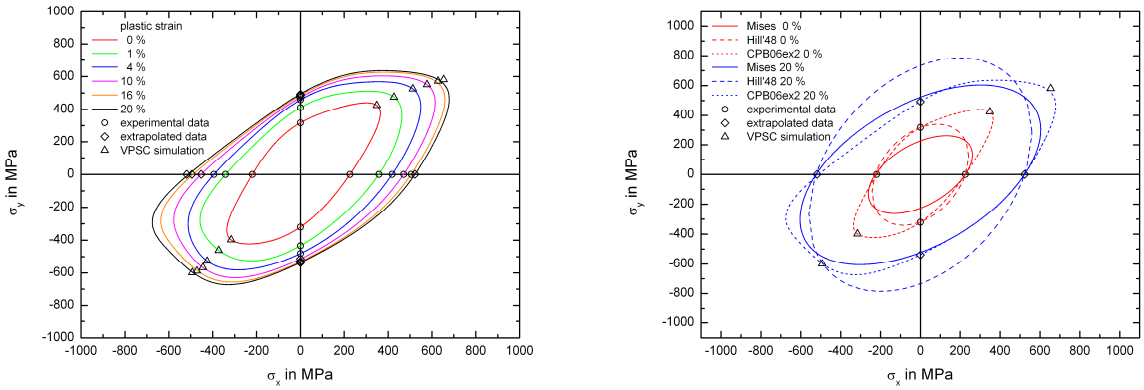

Fig. 14: Yield loci according to CPB06ex2 (left). Yield loci according to Von Mises, Hill and CPB06ex2 (right).

4.2.2 Single element simulation

The yield function presented in section 4.1 has been implemented in a ABAQUS VUMAT by using a cutting plane algorithm. For monotonic uniaxial loadings, single element simulations were performed using a continuum element with eight nodes and reduced integration (ABAQUS type: C3D8R). In each simulation four nodes on one face of the element were constrained in loading direction and the four nodes on the opposite face were given a displacement in either the tensile or compressive direction. The calculated stress-strain curves were compared with the experimental data (Fig. 15 A - C).

A: *Rolling direction*

Compression **Tension**

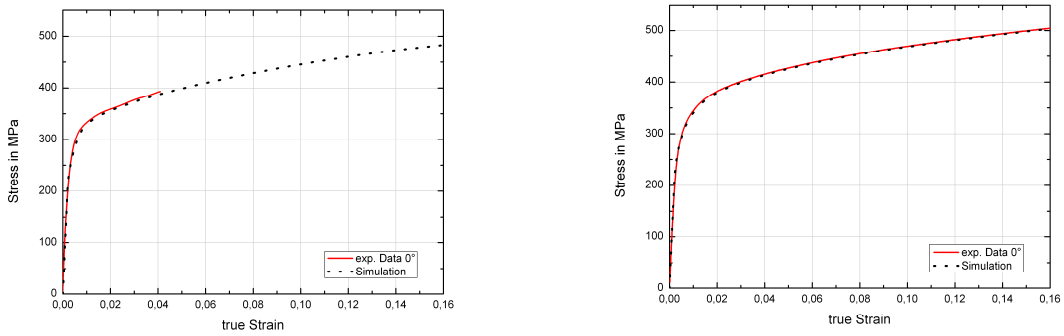

B: *45° direction*

Compression **Tension**

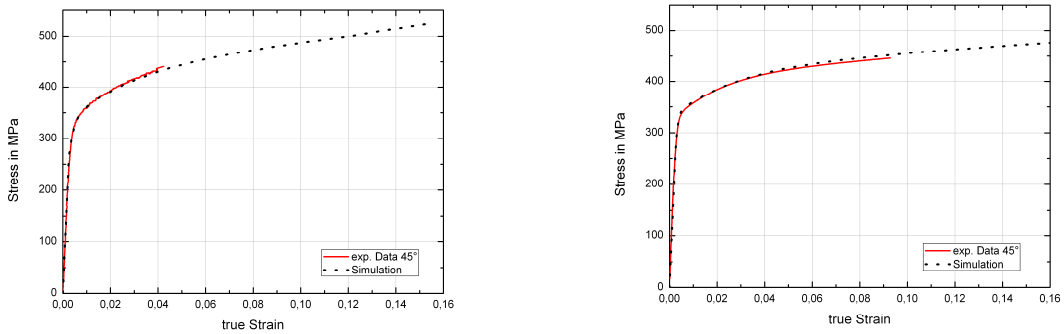

C: *transverse direction*

Compression **Tension**

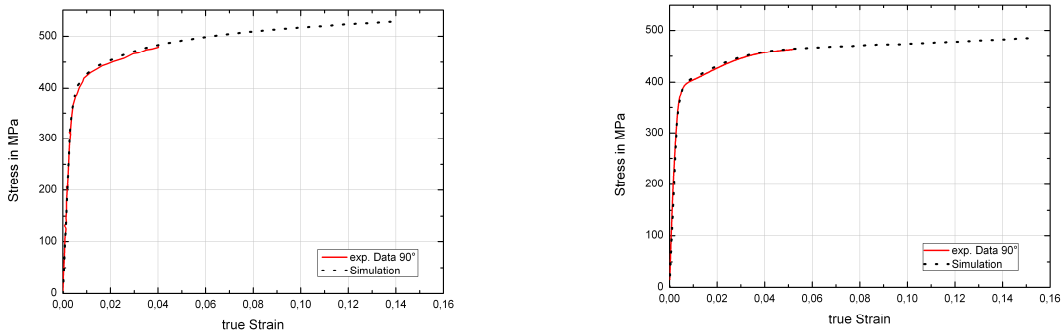

Fig. 15: Comparison between experimental data and simulation results for uniaxial loading in different directions.

It should be noted that the model can describe the experimental data for tensile and compressive loading in all directions very well. Thus, it can reproduce the anisotropic response of the titanium alloy under monotonic loading. In deep drawing processes not only isotropic hardening but also kinematic hardening is relevant, due to cyclic loading. For this reason, the material model is extended for this kind of loading processes.

4.3 Material model for cyclic loading

Especially in deep drawing processes, the material undergoes cyclic deformation in many areas (e.g. drawing radii, drawing bead). Therefore the description of the Bauschinger effect

plays a central role. For this reason, kinematic hardening as a functional of plastic strain is considered to describe cyclic plastic deformation of the material, in addition to the isotropic hardening. One approach to this is the model of Armstrong and Frederick (1966).

4.3.1 Finite plasticity including kinematic hardening

To take kinematic hardening into account, Eq. (11) is replaced by

$$\mathbf{\Sigma} = \mathbf{C} : (\mathbf{S} - \mathbf{X}) \text{ und } \mathbf{\Sigma}^{'} = \mathbf{C}^{'} : (\mathbf{S} - \mathbf{X}) . \tag{17}$$

The backstress tensor **X** is written as a sum of several components (Chaboche and Rousselier, 1983):

$$\mathbf{X} = \sum_{k=1}^{m} \mathbf{X}_k . \tag{18}$$

The evolution equations for the components of the backstress tensor are given by

$$\dot{\mathbf{X}}_k = c_k \hat{\mathbf{D}}_p - b_k \dot{\lambda} \mathbf{X}_k \tag{19}$$

where c_k and b_k are model parameters. The flow potential expands to

$$F(\boldsymbol{\sigma}, \mathbf{X}, \bar{\varepsilon}_{pl}) = \bar{\sigma}(\boldsymbol{\sigma}, \mathbf{X}, \bar{\varepsilon}_{pl}) - Y(\bar{\varepsilon}_{pl}) . \tag{20}$$

The isotropic hardening Y is given by

$$Y(\bar{\varepsilon}_{pl}) = \sigma_y + k_1 \cdot (1 - e^{-k_2 \bar{\varepsilon}_{pl}}) , \tag{21}$$

where σ_y denotes the radius of the yield surface in reference direction (here: rolling direction) at the beginning of plastic yielding. The maximum size of the yield surface in reference direction is defined by k_1, k_2 defines how fast this saturation value is reached as a function of the equivalent plastic strain. The model parameters k_1 and k_2 are fitted together with the parameters of the backstress tensor to cyclic loading tests. Thus, the hardening response of the material is described by seven parameters, when two backstress tensors are used.

4.3.2 Parameter fitting to one load cyclic

The fitted model parameters for the isotropic-kinematic hardening model with two backstresses are shown in Table 6.

Table 6: Fitted model parameters: Fit to experimental data for one load cycle.

isotropic hardening			kinematic hardening			
σ_y	k_1	k_2	c_1	b_1	c_2	b_2
226.26	112.56	12	18000	198	296	5

The model parameters were fitted to the first load cycle of the cyclic loading test and the stress-strain curve from the monotonic tensile test in rolling direction. The consideration of the tensile test is necessary because of the relatively small strain amplitudes achieved in the

cyclic test. Thus, a more accurate description of the hardening at larger strains is possible. Fig. 16 shows the experimental and the fitted tension and tension-compression curves. The small difference between the results of the tension and the tension-compression tests may be explained by the use of two different testing machines.

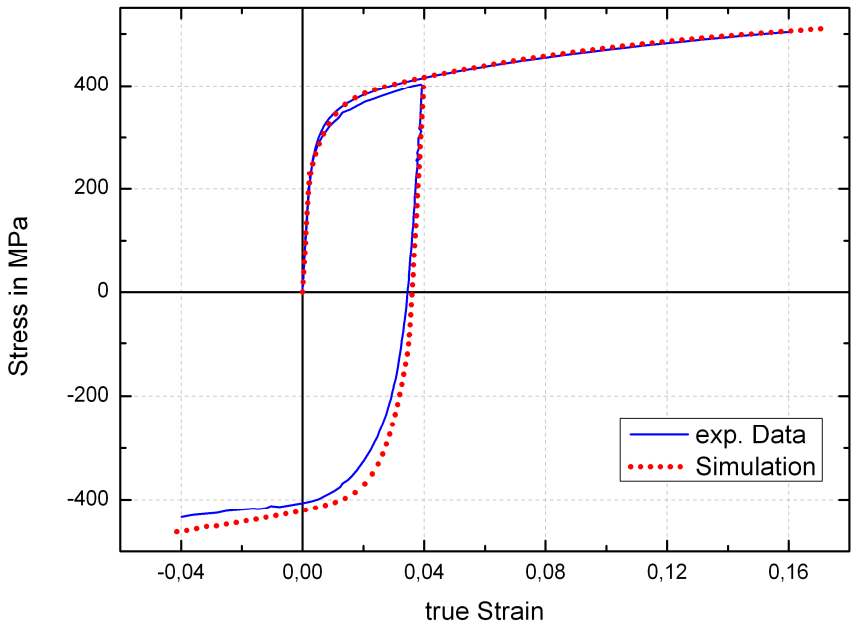

Fig. 16: Experimental and fitted tension and tension-compression curves in rolling direction.

4.3.3 Simulation of strip drawing tests

The strip drawing tests described in section 2.2.4 were simulated with the proposed model and the computed springback was compared with the experimental results. Furthermore, the results were compared with the predictions of simpler models (von Mises and Hill'48) to determine the influence of a more accurate yield model on the springback prediction. It should be noted that kinematic hardening is considered in all those simulations. The simulations were performed using the explicit solver ABAQUS/Explicit. The subsequent elastic springback of the strip was simulated implicitly with ABAQUS/Standard. The strip was discretized with solid elements of ABAQUS type C3D8R.
The friction coefficient between strip and tool was set to $\mu = 0.12$. It is known from previous studies that the Young's modulus has a significant influence on the springback. Since this study is aimed to compare different plasticity models, a unique Young's modulus of E = 116 000 MPa was used for both directions, despite the fact that slightly different moduli were obtained from the starting slopes of the tensile tests (see Table 2).
A comparison of the springback contours of the various models with experimental data is shown in Fig. 17.

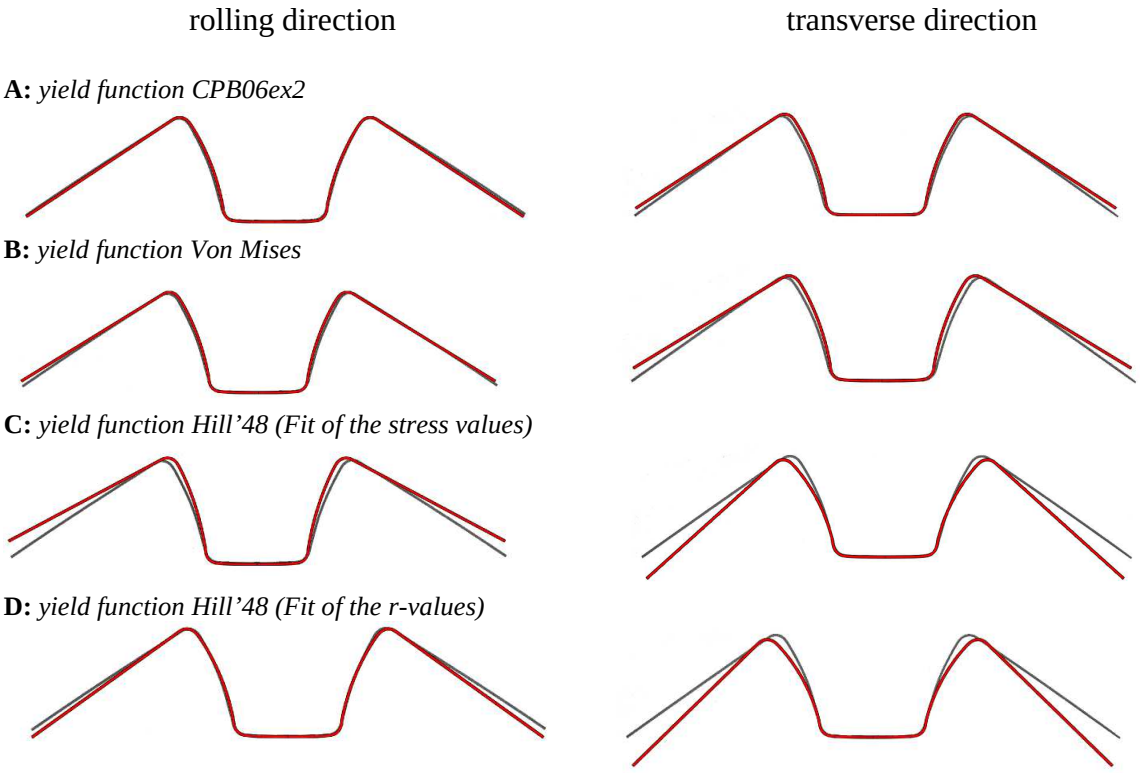

Fig. 17: Comparison between experiment (black) and simulation (red) using different yield functions.

The complex yield function of CPB06ex2 is able to predict the contours in rolling and transverse directions very well (Fig. 17 A). The yield function of von Mises also shows good agreement in rolling direction, but calculates a slightly too large springback in transverse direction (Fig. 17 B). The yield function of Hill'48 delivers inferior results, especially in transverse direction (Fig. 17 C and D).

One reason why the standard von Mises model could reproduce the experimental results with only small deviations could be that there is only little tension-compression asymmetry of the material used (see Fig. 6 and 7). In addition, it can be seen from Fig. 14 (right) that both the von Mises model and the CPB06ex2 model describe the available experimental data points in the principal directions $\sigma_x = 0$ and $\sigma_y = 0$ almost equally well. These are the predominant loading directions in the strip drawing tests evaluated here.
The clearly insufficient results from the Hill'48 model correspond with the large deviation of the yield locus from the data points (see Fig. 14 right). Particularly in transverse direction, the differences are quite large.
The analyzed results demonstrate the superiority of the new model over the standard models. The fact that the von Mises model also gives very reasonable results may be explained by the almost identical predictions of the yield surface in the rolling direction in Fig. 14. However, it can be seen that in transverse direction the von Mises model can predict the shape less well. This can be explained by the deviation of the yield locus at small strains in transverse direction (see Fig. 14).
It might be concluded that the strip drawing test with in principle uniaxial loading is not well suited to discriminate between the CPB06ex2 and the von Mises model. In many real drawing processes, however, the stress-strain histories are much more complex and far away from the uniaxial state. Therefore, the advantages of the complex CPB06ex2 model over the other models must be proven in further investigations.

5. Conclusions

In this work, extensive experimental studies on the deformation response of titanium alloy Ti-X were carried out. In addition to standard tension, compression and tension-compression tests, the texture was determined using EBSD. For the validation of the model used, strip drawing tests were available.
In the experimental results the tension-compression asymmetry, typical for titanium materials and the anisotropy can be observed. The occurrence of the tension-compression asymmetry is due to different deformation modes which are activated differently depending on the loading direction; i.e. under compression loading there is twinning while under tension there is no twinning. Based on the findings of the experiments an anisotropic yield function (CPB06ex2 from Plunkett et al., 2008) has been chosen, which is able to describe the features of the observed material response. By evolution of the model parameters as a function of equivalent plastic strain, anisotropic hardening could be described. The simulation of monotonic loadings shows that this model is able to reproduce the anisotropic hardening behavior with great accuracy. In a further step the model was extended to include the Bauschinger effect. This is of great importance for the springback simulation. The finite element simulations of strip drawing tests agree very well with the experimental results.
The models used so far do not take into account the influence of the strain rate. However, it is known that especially titanium alloys have a strong strain rate dependency (see for example Khan et al., 2004, 2007, Chichili et al., 1998). For this reason there is a great interest in the extension of the present model.

Acknowledgements

The authors wish to thank Dr. Winfried Schmitt and Prof. Dr. Hermann Riedel from Fraunhofer-Institute for Mechanics of Materials IWM, Germany for the detailed discussions and helpful comments related to this work.

References

Armstrong P.J., Frederick C.O.: A mathematical representation of the multiaxial Bauschinger effect. C.E.G.B. Report RD/B/N 731, Berkley Nuclear Laboratories (1966).

Boyer,R.; Welsch, G. and Collings E.W. (ed.) Materials Properties Handbook: Titanium Alloys, ASM International, Metals Park (OH) (1994).

Cazacu O., Barlat F., 2001, Generalization of Drucker's yield criterion to orthotropy, Mathematics and Mechanics of Solids 6, 613-630.

Cazacu O., Barlat F., 2003, Application of the theory of representation to describe yielding of anisotropic aluminum alloys. Int. J. Eng. Sci. 41, 1367-1385.

Cazacu O., Barlat F., 2004, A criterion for description of anisotropy and yield differential effects in pressure-insensitive metals. Int. J. Plasticity 20, 2027-2045.

Cazacu O., Plunkett B., Barlat F., 2006, Orthotropic yield criterion for hexagonal closed packed metals, Int. J. Plasticity 22, 1171-1194.

Chaboche J.L., Rousselier G., 1983, On the plastic and viscoplastic constitutive equations - Part I. Rules developed with internal variable concept, Journal of Pressure Vessel Technology 105, p. 153-158.

Chichili D.R., Ramesh K.T., Hemker K.J., 1998, The high-strain-rate response of alpha-titanium: experiments, deformation mechanisms and modeling, Acta mater. Vol. 46, No. 3, pp. 1025-1043.

Follansbee P.S., Gray G.T., 1989, An analysis of the low temperature, low and high strain-rate deformation of Ti-6Al-4V, Metallurgical Transactions A 20, 863-874.

Han C.-S., Chung K., Wagoner R.H., Oh S.-I., 2003, A multiplicative finite elasto-plastic formulation with anisotropic yield functions, Int. J. Plasticity 19, 197-211.

Hora P., Modellierung des Kaltverfestigungsverhaltens bei metallischen Werkstoffen, Conference, Freiberg, 2011.

Kahn A.S., Huang S., 1995, Continuum Theory of Plasticity. John Wiley & Sons.

Kahn A.S., Suh Y.S., Kazmi R., 2004, Quasi-static and dynamic loading responses and constitutive modeling of titanium alloys, Int. J. Plasticity 20, 2233-2248.

Kahn A.S., Kazmi R., Farrokh B., 2007, Multiaxial and non-proportional loading responses, anisotropy and modeling of Ti-6Al-4V titanium alloy over wide ranges of strain rates and temperatures, Int. J. Plasticity 23, 931-950.

Krasovskyy A.: Verbesserte Vorhersage der Rückfederung bei der Blechumformung durch weiterentwickelte Werkstoffmodelle, 2005.

Lebensohn R.A., Tomé C.N., 1993, A self-consistent anisotropic approach for the simulation of plastic deformation and texture development of polycrystals: Application to zirconium alloys. Acta metall. mater. Vol. 41, No.9, pp. 2611-2624

Lecomte J.S., Philippe M.J., Klimanek P., 1997, Plastic deformation of a Ti-6% Al-4% V alloy with strong transverse-type crystallographic α-texture at elevated temperatures, Materials Science and Engineering A234-236, 869-872.

Majorell A., Srivatsa S., Picu R.C., 2002, Mechanical behavior of Ti-6Al-4V at high and moderate temperatures - Part I: Experimental results, Materials Science and Engineering A326, 297-316.

Majorell A., Srivatsa S., Picu R.C., 2002, Mechanical behavior of Ti-6Al-4V at high and moderate temperatures - Part II: constitutive modeling, Materials Science and Engineering A326, 306-316.

Nemat-Nasser S., Guo W.G., Cheng J.Y., 1999, Mechanical properties and deformation mechanisms of commercially pure titanium. Acta mater. Vol.47, No. 13, pp. 3705-3720.

Nemat-Nasser S., Guo W.G, Nesterenko V.F., Indrakanti S.S., Gu Y.-B., 2001, Dynamic response of conventional and hot isostatically pressed Ti-6Al-4V alloys: experiments and modeling, Mechanics of Materials 33, 425-439.

Nixon M.E., Cazacu O., Lebensohn R.A., 2010, Anisotropic response of high-purity α-titanium: Experimental characterization and constitutive modeling, Int. J. Plasticity 26, 516-532.

Plunkett B., Lebensohn R.A., Cazacu O., Barlat F., 2006, Anisotropic yield function of hexagonal materials taking into account texture development and anisotropic hardening, Acta Mat. 54, 4159-4169.

Plunkett B., Cazacu O., Barlat F., 2008, Orthotropic yield criteria for description of the anisotropy in tension and compression of sheet metals, Int. J. Plasticity 24, 847-866.

Seshacharyulu T., Medeiros S.C., Frazier W.G., Prasad Y.V.R.K., 2000, Hot working of commercial Ti-6Al-4V with an equiaxed α-β microstructure: materials modeling considerations, Materials Science and Engineering A284, 184-194.

Seshacharyulu T., Medeiros S.C., Frazier W.G., Prasad Y.V.R.K., 2002, Microstructural mechanisms during hot working of commercial grade Ti-6Al-4V with lamellar starting structure, Materials Science and Engineering A325, 112-125.

Wu P.D., Jain M., Savoie J., MacEwen S.R., Tugcu P., Neale K.W., 2003, Evaluation of anisotropic yield functions for aluminum sheets, Int. J. Plasticity 19, 121-138.

Yapici G.G., Karaman I., Luo Z.-P., 2006, Mechanical twinning and texture evolution in severely deformed Ti-6Al-4V at high temperatures, Acta Materialia 54, 3755-3771.